Chemistry–A European Journal

Research Article
doi.org/10.1002/chem.202300579

Chemistry Europe
European Chemical Societies Publishing

www.chemeurj.org

Engineering the BASHY Dye Platform toward Architectures with Responsive Fluorescence

João Felicidade,[a] Fabio M. F. Santos,[a] Jesús F. Arteaga,[b] Patricia Remón,[b] René Campos-González,[b] Ha-Chi Nguyen,[c] Francisco Nájera,[d, e] Francisco Boscá,[f] David Y. W. Ng,[c] Pedro M. P. Gois,*[a] and Uwe Pischel*[b]

Abstract: A set of nine boronic-acid-derived salicylidenehydrazone (BASHY) complexes has been synthesized in good to very good chemical yields in a versatile three-component reaction. In an extension to previous reports on this dye platform, the focus was put on the electronic modification of the "vertical" positions of the salicylidenehydrazone backbone. This enabled the observation of fluorescence quenching by photoinduced electron transfer (PeT), which can be reverted by the addition of acid in organic solvent (OFF-ON fluorescence switching). The resulting emission is observed in the green-to-orange spectral region (maxima at 520–590 nm). In contrast, under physiological pH conditions in water, the PeT process is inherently decativated, thereby enabling the observation of fluorescence in the red-to-NIR region (maxima at 650–680 nm) with appreciable quantum yields and lifetimes. The latter characteristic supported the application of the dyes in fluorescence lifetime imaging (FLIM) of live A549 cells.

Introduction

The quest for organic fluorophores whose photophysical properties can be flexibly fine-tuned by means of the straightforward synthetic manipulation of their electronic properties is an evergreen topic of modern dye chemistry.[1–12] In the context of innovative fluorescent organoboron architectures[1,2,13–22] we developed recently the modular platform of boronic-acid derived salicylidenehydrazone (BASHY) complexes.[23,24] These fluorescent dyes show an interesting combination of an intramolecular charge-transfer (ICT) mechanism[23] and cyanine-like behavior[25,26] and have revealed promising potential for bioimaging applications.[23,26–29] The dyes are generated in a synthetically flexible and robust multicomponent reaction,[23,26] opening manifold possibilities for the electronic manipulation of the BASHY skeleton.[24]

Having previously established that the fluorescence properties of BASHY dyes are founded on the "horizontal" donor-π-acceptor (D-π-A) architecture (red D and blue A in Figure 1) and its π-conjugation length,[23,24,26] we herein focus our attention on the electron-donor substitution at the "vertical" positions (green and cyan in Figure 1), principally using NEt_2. This design option was guided by the anticipation that this may enable photoinduced electron transfer (PeT) quenching, leading to pH-controlled OFF-ON switching of the fluorescence of the dyes.[30–32] This would significantly enrich the functional toolbox of the BASHY family with view on the further optimization for bioimaging applications.

[a] J. Felicidade, Dr. F. M. F. Santos, Prof. Dr. P. M. P. Gois
Research Institute for Medicines (iMed.ULisboa)
Faculty of Pharmacy, Universidade de Lisboa
Av. Prof. Gama Pinto, 1649-003 Lisbon (Portugal)
E-mail: pedrogois@ff.ulisboa.pt
Homepage: https://sites.ff.ulisboa.pt/goislab/

[b] Prof. Dr. J. F. Arteaga, Dr. P. Remón, R. Campos-González, Prof. Dr. U. Pischel
CIQSO – Centre for Research in Sustainable Chemistry and Department of Chemistry
University of Huelva
Campus de El Carmen s/n, 21071 Huelva (Spain)
E-mail: uwe.pischel@diq.uhu.es
Homepage: https://uhu-ciqso.es/organic-synthesis-and-photochemistry-laboratory/

[c] H.-C. Nguyen, Dr. D. Y. W. Ng
Max Planck Institute for Polymer Research
Ackermannweg 10, 55128 Mainz (Germany)

[d] Prof. Dr. F. Nájera
Departamento de Química Orgánica
Universidad de Málaga
Campus Teatinos s/n, 29071 Málaga (Spain)

[e] Prof. Dr. F. Nájera
Instituto de Investigación Biomédica de Málaga y Plataforma en Nanomedicina – IBIMA
Plataforma Bionand
Parque Tecnológico de Andalucía, 29590 Málaga (Spain)

[f] Dr. F. Boscá
Instituto de Tecnología Química
Universitat Politècnica de València – Consejo Superior de Investigaciones Científicas
Avda. de los Naranjos s/n, 46022 Valencia (Spain)

Supporting information for this article is available on the WWW under https://doi.org/10.1002/chem.202300579

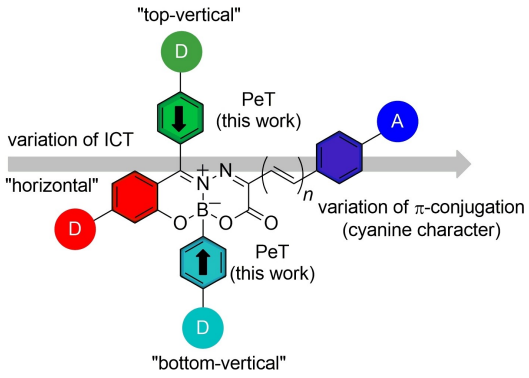

Figure 1. General structure of the cross-substituted BASHY dyes and potentially implicated excited state pathways; D = donor, A = acceptor.

Results and Discussion

Synthesis

Based on different combinations of regiospecific substitution, a small library of nine cross-substituted BASHY dyes was prepared in good to very good yields (generally 70–85%; see the Experimental Section for details) in a three-component reaction (3CR; Scheme 1). This procedure involves a hydrazone component, an α-keto carboxylic acid, and an arylboronic acid.[23,33–35] The synthesis of commercially non-available precursors is described in the Supporting Information. The resulting BASHY dyes **1**–**9** (see structures in Scheme 1) were characterized by ^{1}H and ^{13}C NMR spectroscopy, IR spectroscopy, as well as by mass spectrometry (see data in Experimental Section and copies of the spectra in the Supporting Information).

UV/vis absorption and fluorescence in organic medium

The photophysical key data in nonpolar toluene and polar acetonitrile are summarized in Table 1 (see also representative spectra in Figure 2 as well as in the Supporting Information). Starting the structure-property analysis with the dyes that lack an electron donor in the "top-vertical" position (i.e., **1**, **6**, and **8**), some general trends can be identified: a) the maxima of the long-wavelength absorption band and of the emission spectrum are bathochromically shifted with increasing π-conjugation along the salicylidenehydrazone backbone and b) the Stokes shift is increased in polar solvents. These observations corroborate the dual cyanine-like and ICT character of the dyes,[23,26] with an emphasis on nonpolar and polar media, respectively. The dyes **1**, **6**, and **8** maintain appreciable fluorescence quantum yields (Φ_f) of up to 0.17 in toluene and 0.15 in acetonitrile. This is notable, especially when taking into account that they emit in the orange-to-red spectral window in polar medium, where commonly non-radiative deactivation exerts a competitive role in accordance with the energy-gap law. While these quantum yields are not extraordinarily high, this is effectively counterbalanced by the large molar absorption coefficient (ca. 50 000–60 000 $M^{-1}cm^{-1}$), which promotes a significant brightness of the dyes ($\varepsilon \times \Phi_f$ up to ca. 10 000 $M^{-1}cm^{-1}$).

The situation described above changes for the installation of electron-donor substitution in the "top-vertical" position (green in Figure 1), for example, an additional NEt_2 group in **2**, **7**, and **9**. To our initial surprise this did not lead to further bathochromic shifts in the UV/vis-absorption and fluorescence spectra. *Ad hoc* it cannot be excluded that the "top-vertical" position would be electronically communicated with the ligand by conjugation. Hence, the installation of the additional electron donor on the same end as the "horizontal" NEt_2 donor could potentially lead to additional ICT and further shifts of the emission towards the deep-red spectral window. While theoretical calculations (see below) support the correct structural

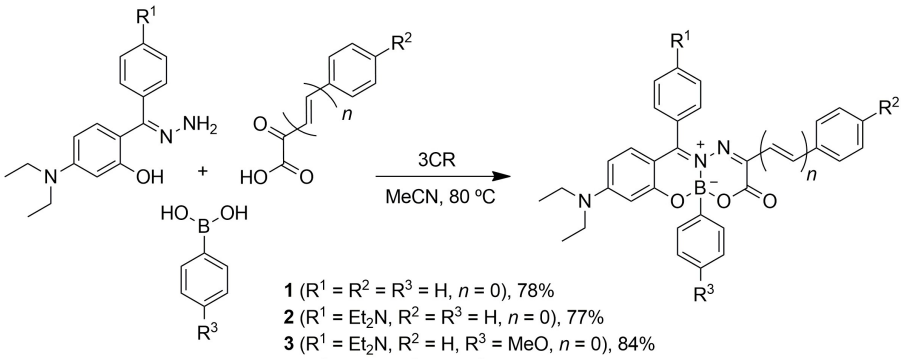

1 ($R^1 = R^2 = R^3 = H$, $n = 0$), 78%
2 ($R^1 = Et_2N$, $R^2 = R^3 = H$, $n = 0$), 77%
3 ($R^1 = Et_2N$, $R^2 = H$, $R^3 = MeO$, $n = 0$), 84%
4 ($R^1 = Et_2N$, $R^2 = H$, $R^3 = Et_2N$, $n = 0$), 70%
5 ($R^1 = Et_2N$, $R^2 = CN$, $R^3 = H$, $n = 0$), 30%
6 ($R^1 = R^2 = R^3 = H$, $n = 1$), 70%
7 ($R^1 = Et_2N$, $R^2 = R^3 = H$, $n = 1$), 85%
8 ($R^1 = R^2 = R^3 = H$, $n = 2$), 60%
9 ($R^1 = Et_2N$, $R^2 = R^3 = H$, $n = 2$), 80%

Scheme 1. 3CR for the formation of the BASHY dyes **1**–**9**.

Table 1. UV/vis-absorption and fluorescence properties of the dyes **1**–**9** in toluene and acetonitrile.[a]

					Toluene				Acetonitrile			
	R^1	R^2	R^3	*n*	λ_{abs} [nm] (ε [$M^{-1}cm^{-1}$])	λ_f [nm]	Φ_f[b]	τ_f [ns][c]	λ_{abs} [nm] (ε [$M^{-1}cm^{-1}$])	λ_f [nm]	Φ_f[b]	τ_f [ns][c]
1	H	H	H	0	480 (58000)	521	0.17	0.74	481 (56000)	546	0.08	0.60
2	Et_2N	H	H	0	478 (71000)	522	0.06	0.78	478 (63000)	–	–	–
2H$^+$[d]									485	553	0.04	0.41
3	Et_2N	H	MeO	0	478 (54000)	522	0.06	0.79	477 (52000)	–	–	–
4	Et_2N	H	Et_2N	0	475 (56000)	–	–	–	476 (55000)	–	–	–
4H$^+$[d]									484	548	0.02	0.36
5	Et_2N	CN	H	0	491 (47000)	581	0.02	2.09	487 (45000)	–	–	–
6	H	H	H	1	504 (65000)	542	0.09	0.75	507 (61000)	574	0.15	1.46[e]
7	Et_2N	H	H	1	501 (66000)	540	0.03	0.52	499 (60000)	–	–	–
7H$^+$[d]									512	572	0.09	1.22[e]
8	H	H	H	2	521 (73000)	562	0.05	0.53	519 (54000)	584	0.11	1.32[e]
9	Et_2N	H	H	2	498 (61000)	559	0.05	0.44	510 (65000)	–	–	–
9H$^+$[d]									527	592	0.10	1.11[e]

[a] The measurements were done with air-equilibrated solutions. The assignment of the moieties R^1, R^2, and R^3 as well as *n* is shown in Scheme 1. "-" denotes that no fluorescence was observed ($\Phi_f < 0.001$). [b] The emission quantum yields were measured relative to *N*-propyl-4-amino-1,8-naphthalimide as reference ($\Phi_f = 0.48$ in acetonitrile); Ref. [23]. [c] The emission lifetimes of the major component (>90% weight) are given, except where indicated otherwise. [d] Generated by addition of 10 equiv. CH_3SO_3H (dyes **2**, **7**, and **9**) or 20 equiv. CH_3SO_3H (dye **4**). [e] The average lifetime is given, where the major component of a biexponential decay has a weight of ≤90%.

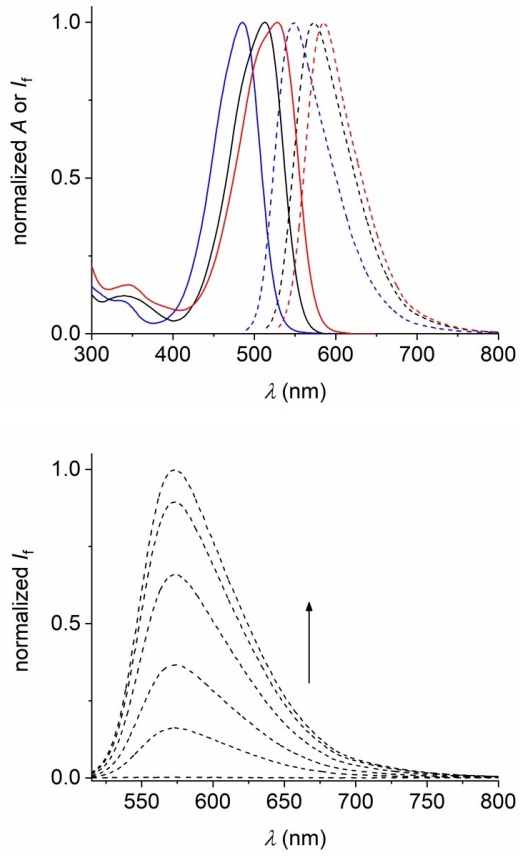

Figure 2. Top: UV/vis absorption (solid) and fluorescence (dashed) spectra of the dyes **2** (blue), **7** (black), and **9** (red) in the presence of 10 equiv. CH_3SO_3H in acetonitrile (dye concentration 5 μM). Bottom: Fluorescence spectra of **7** in acetonitrile upon addition of increasing amounts of CH_3SO_3H. Note that the initial fluorescence of the dye is barely observable.

positioning of the "vertical" electron donor, the frontier orbital analysis and the observed absence of further bathochromic shifts of the optical spectra exclude such mechanistic scenario.

Although additional ICT from the "top-vertical" position is excluded, a PeT mechanism could be still operative. In this respect it is noteworthy, that especially the dyes **2** and **7** show already some degree of fluorescence quenching in nonpolar toluene in comparison to their counterparts **1** and **6** (lacking an electron-donor substituent in the "top-vertical" position). In the more polar acetonitrile, where PeT would thermodynamically more favored, hardly any fluorescence is seen for **2**, **7**, and **9** ($\Phi_f < 0.001$). However, significant fluorescence intensity can be restored by protonation with methanesulfonic acid (CH_3SO_3H), which deactivates the electron-donor properties of the "top-vertical" NEt_2 substituent (see Figure 2 for spectra of protonated dyes and titration of **7** with acid). Hence, fluorescence quenching by PeT is hindered, which translates especially for the dyes **7** and **9** into a dramatic fluorescence enhancement with factors of at least 90 on addition of 10 equivalents of acid. Noteworthy, the same amount of acid had no effect on the UV/vis-absorption or fluorescence of the dyes **1**, **6**, and **8**, confirming that the "top-vertical" NEt_2 moiety (green in Figure 1) is protonated. This underpins the strongly reduced basic character of the NEt_2 group that is attached to the "horizontal" axis (red in Figure 1) of the salicylidenehydrazone, being involved in ICT along the ligand backbone.[23,24]

Considering the dyes where in addition to the electron-donor substitution in the R^1 position also the R^2 and R^3 positions were electronically variable (dyes **3**–**5**), the following observations can be made. The installation of a strong electron acceptor (i.e., CN) at the R^2 position (blue in Figure 1) leads to a further bathochromic shift of the absorption and emission spectra (compare **5** with **2**). This is in agreement with increased charge-transfer along the salicylidenehydrazone axis, as previously shown for related dyes.[23,24] Electron-donating substituents in the R^3 position (cyan in Figure 1) do not lead to any

significant spectral changes. However, additional fluorescence quenching is observed even in the nonpolar toluene, to the point that dye **4** is hardly emissive in any of the solvents. Noteworthy, the sp^3-hybridized boron forces a tetrahedral geometry and this positions the "bottom-vertical" phenyl ring (cyan in Figure 1) out of the plane of the salicylidenehydrazone backbone, hampering ICT by the impossibility of mesomeric conjugative electronic effects. Hence, PeT is reasonably assumed to be operative as fluorescence quenching mechanism, involving the R^3 electron donor.

Transient absorption

Nanosecond transient absorption studies in acetonitrile were undertaken to gain further insights into the excited-state behavior of the dyes **7** and **9**. While the transient signals for the dyes were very weak in the absence of acid, protonation led to highly defined spectra (see Table 2 and Figure 3 for dye **9** in the presence of acid). Directly after the laser flash both dyes show a negative signal between 440 and 570 nm, which resembles the inverted long-wavelength absorption features. Hence, this transient signal is assigned to the ground-state bleaching. Further, a positive broad signal with a maximum around 660–670 nm was observed. This one is attributed to the excited triplet state (triplet-triplet absorption). This assignment is based on three key observations: a) the long lifetime (24–26 μs), b) the quenching by oxygen (k_q ca. $3.5\times10^9\ M^{-1}\,s^{-1}$), and c) the appearance of the same signal by triplet-energy-transfer sensitization with benzophenone as donor (see the Supporting Information). The fact that the transient signals become more pronounced in the presence of methanesulfonic acid (10 equiv.), especially for dye **9** (see amplitudes of the kinetic decays shown in the inset of Figure 3), is a consequence of the blocked PeT deactivation of the precursor excited singlet state (see fluorescence data above). The quantum yield for excited triplet state formation via intersystem crossing (ISC) was determined as $\Phi_{ISC}\approx0.53$ for protonated **9** and 0.05 for protonated **7**. The latter protonated dye, which has considerably more ICT character than **9** (see below), seems not to populate the triplet state to a significant extent. Likely the ICT state acts as energy sink, making ISC energetically less likely.

Table 2. Laser-flash photolysis data for **7** and **9** in deaerated acetonitrile (excitation at 340 nm, unless noted otherwise).

	Φ_T[a]	ε [$M^{-1}cm^{-1}$][a]	$\lambda_{T\text{-}T}$ [nm]	τ [μs][b]
7	<0.01	13500	670	n.d.
7 (+ acid)[c]	0.05	13500	670	26
9	≈0.02	12800	670	n.d.
9 (+ acid)[c]	0.53	12800	670	24

[a] The triplet quantum yield (Φ_T) and the molar absorption coefficient (ε) of the T–T absorption at 670 nm were determined with benzophenone in acetonitrile as reference ($\Phi_T=1$; $\varepsilon_{525\,nm}=6500\ M^{-1}cm^{-1}$).[36] [b] Excitation at 510 nm. [c] Presence of 10 equiv. CH_3SO_3H. n.d.: not determined due to the low signal.

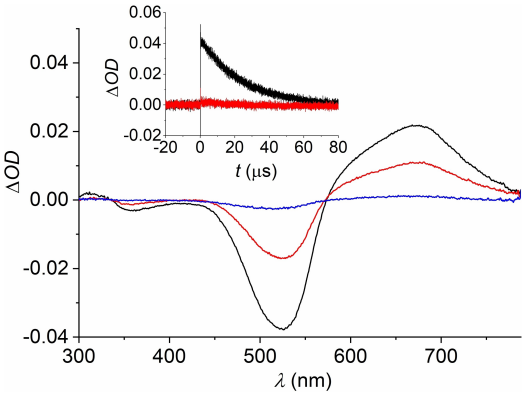

Figure 3. Nanosecond laser-flash photolysis ($\lambda_{ex}=510$ nm) of dye **9** (10 μM) in the presence of 10 equiv. CH_3SO_3H in deaerated acetonitrile. The transient spectra correspond to time zero (black) as well as 15 (red) and 60 μs (blue) after the laser flash. The inset shows the decay of the signal at 660 nm in the presence of 10 equiv. CH_3SO_3H (black) and the absence of acid (red). Note that the kinetic traces were recorded for $\lambda_{ex}=350$ nm.

Theoretical calculations

In order to obtain additional insight into the electronic nature of these dyes, density functional theory calculations at the LC-wHPBE/6-311++G(2d,p) level of theory[37] were performed on **1**, **2**, **7**, and **9** (Table 3, Figure 4, and the Supporting Information). This allowed conclusions about the role of the "top-vertical" electron-donor substitution and the π-conjugation length of the ligand backbone. The ICT character of the dyes was judged by the charge-transfer index (D_{CT}), being the distance between barycenters of density variation. This parameter is largest for **1** and **2**, that is, 1.826 and 1.974 Å, respectively. Noteworthy, the "top-vertical" NEt_2 donor in **2** seems not to trigger significant additional ICT. This is in line with the experimentally observed invariance of the spectral features between **1** and **2**. However, on extension of the backbone by exocyclic double bonds, the ICT character along the horizontal ligand backbone is gradually diminished ($D_{CT}=$ 1.491 and 0.929 for **7** and **9**, respectively). Consequently the cyanine-like character is increasingly emphasized (Table 3), providing characteristics of a locally excited (LE) state. This is especially the case for **9**.

Table 3. Charge-transfer indices for **1**, **2**, **7**, and **9** at the PCM(ACN)/LC-wHPBE/6-311++G(2d,p)//PCM(ACN)/LC-wHPBE/6-31G(d) level of theory.

Cmpd	D_{CT} [Å][a]	μ_{CT} [D][b]	Δr_{S1} [Å][c]	Observation[d]
1	1.826	5.644	2.831	ICT
2	1.974	6.392	2.382	ICT
7	1.491	4.712	2.003	ICT/LE
9	0.929	2.903	1.744	LE

[a] D_{CT}: Charge transfer index (distance between barycenters of density variation). [b] μ_{CT}: variation of the dipole moment associated to charge transfer. [c] The index Δr_{S1} relies on the centroids of the orbitals involved in the excitation (based on the positions of the hole and the electron). The Δr_{S1} index is a quantitative indicator for measuring charge-transfer length of electron excitation. [d] $\Delta r_{S1}>2$ implies an ICT (intramolecular charge transfer) state and a $\Delta r_{S1}<2$ indicates an LE (locally excited) state.[38]

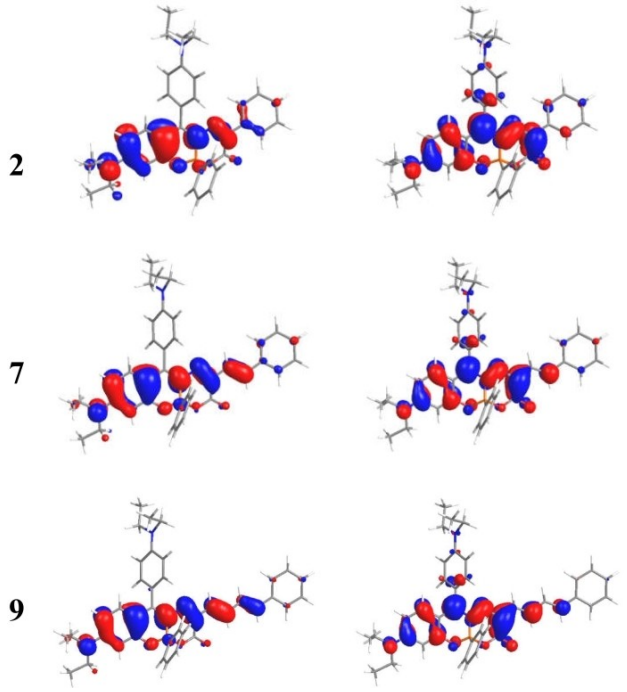

Figure 4. Plots of natural transition orbitals (NTOs; left: hole, right: electron) involved in the $S_1 \leftarrow S_0$ transition of **2**, **7**, and **9**. The weight of the NTOs in the description of the $S_1 \leftarrow S_0$ transition is 94, 92, and 89% for **2**, **7**, and **9**, respectively.

The lowest energy transition ($S_1 \leftarrow S_0$) in **1** is clearly dominated by the LUMO←HOMO transition, with the HOMO being mainly located on the electron-donor moiety (red D in Figure 1) and the LUMO involving the carboxylic group on the acceptor side; see the Supporting Information. This is in accordance with the established ICT character of BASHY dyes.[23] The picture changes for **2** where now the HOMO is strongly manifested at the "top-vertical" *N*,*N*-diethylaminophenyl moiety, while the HOMO-1 additionally implies the "horizontal" NEt_2 donor unit (see the Supporting Information). The LUMO again involves the carboxylic group. The $S_1 \leftarrow S_0$ transition of **2** features principally the LUMO←HOMO-1 (68%) contribution, beside a minor participation from LUMO←HOMO (13%). In order to simplify this picture the analysis of the natural transition orbitals (NTO) is indicated (Figure 4).[39] The hole and electron NTOs of **2** point to an electronic redistribution along the "horizontal" axis, leaving the "top-vertical" *N*,*N*-diethylaminophenyl moiety as bystander (see the Supporting Information). As for **1**, this hints on significant ICT character for **2**, involving mainly push-pull features of the "horizontal" ligand backbone. Hence, once more we infer that the observed fluorescence quenching (see above), caused by the "top-vertical" electron donor (green in Figure 1), is due to PeT rather than ICT.

The $S_1 \leftarrow S_0$ transition in **9** is dominated by the LUMO← HOMO contribution, involving exclusively the "horizontal" axis (see the Supporting Information). The frontier orbitals are spread out along this axis, pointing to a significant contribution of a LE state, in accordance with the cyanine-like character of **9**. The same picture is confirmed by the NTO analysis (Figure 4), demonstrating clearly the absence of electronic involvement of the "top-vertical" NEt_2 electron donor in the spectral properties of the dye. Finally, the electronic characteristics of **7** point to a mixed ICT/LE character, as predicted by the calculated charge transfer indices (Table 3). The $S_1 \leftarrow S_0$ transition receives contributions from the LUMO←HOMO-1 (66%) and LUMO←HOMO (16%). The picture for the HOMO and HOMO-1 is very comparable to that discussed for **2**. However, the LUMO is now much more spread out along the ligand backbone, akin to the observations made for **9**. Again the NTO analysis points to the electronic decoupling of the "top-vertical" electron donor from the rest of the molecule and hence, the $S_1 \leftarrow S_0$ transition is solely guided by the electronic features of the "horizontal" ligand backbone.

Photophysical properties in water

With view on potential applications of the BASHY dyes in bioimaging, their photophysical properties in aqueous solution were determined (Table 4 and Figure 5). For this study **2**, **7**, and **9** were selected, because these dyes showed in acetonitrile the most pronounced response on addition of acid. The study was performed in 10 mM phosphate-buffered saline (PBS; pH 7.4), containing a small amount of *N*,*N*-dimethylformamide (5 vol%) as co-solvent to aid the solubility of the compounds. Noteworthy, the dyes are reasonably stable against hydrolytic decomposition under the chosen experimental conditions (e.g.,

Table 4. Photophysical properties of the dyes **2**, **7**, and **9** in PBS solution.

	λ_{abs} [nm] [ε ($M^{-1}cm^{-1}$)]	λ_f [nm]	Φ_f	τ_f [ns]
2	477 [40000]	652	0.01	1.48
7	494 [42000]	670	0.01	1.28
9	508 [46000]	683	0.01	0.85

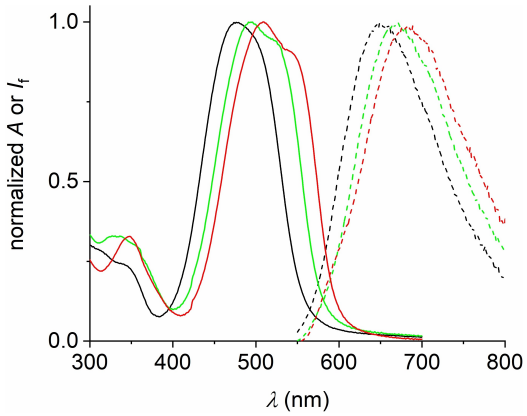

Figure 5. UV/vis absorption (solid lines) and fluorescence (dashed lines) spectra of the dyes **2** (black), **7** (green), and **9** (red) in phosphate-buffered saline (10 mM, pH 7.4). The emission spectra were obtained by excitation of the dyes at their absorption maximum.

after ca. 1 h dye **9** suffered only 5% degradation, monitored by UV/vis absorption spectroscopy; see the Supporting Information).

In comparison to acetonitrile the maxima of the longest-wavelength absorption bands show hardly any variation in aqueous solution and follow the same trend of a bathochromic shift on extension of the π-conjugation. A small long-wavelength tailing was noted for all three dyes, hinting on a minor amount of aggregation. However, as opposed to the unprotonated dyes in acetonitrile, in PBS significant fluorescence (Φ_f ca. 0.01) was observed. In addition, the fluorescence maxima in aqueous solution are significantly red-shifted by about 100 nm as compared to acetonitrile. This can be reasoned with the additional stabilization of the emissive ICT state by water. Hence, the fluorophores emit now deep into the red spectral window (dyes **2** and **7**) or even close to the near-infrared region (dye **9**). Lower fluorescence quantum yields are typically observed for such low-energy emissions due to the action of the energy-gap law, which predicts considerable competition by non-radiative deactivation channels. The fluorescence lifetimes were measured as 850 ps to 1.5 ns (Table 3). However, contrary to the observations made in acetonitrile, the addition of acid to dye solutions in non-buffered water does not lead to a further fluorescence increase. This is reasoned with the possibility of hydrogen-bonding of water to the "top-vertical" NEt_2 group, thereby involving the N lone pair and deactivating PeT already in the absence of acid.

Photophysical characterization in cells

The observation of fluorescence with appreciable lifetimes in aqueous medium encouraged us to test some of the dyes (**2**, **7**, and **9**) in confocal fluorescence lifetime imaging (FLIM). The dyes were incubated with A549 lung adenocarcinoma epithelial cells (Figure 6). Compared to conventional confocal

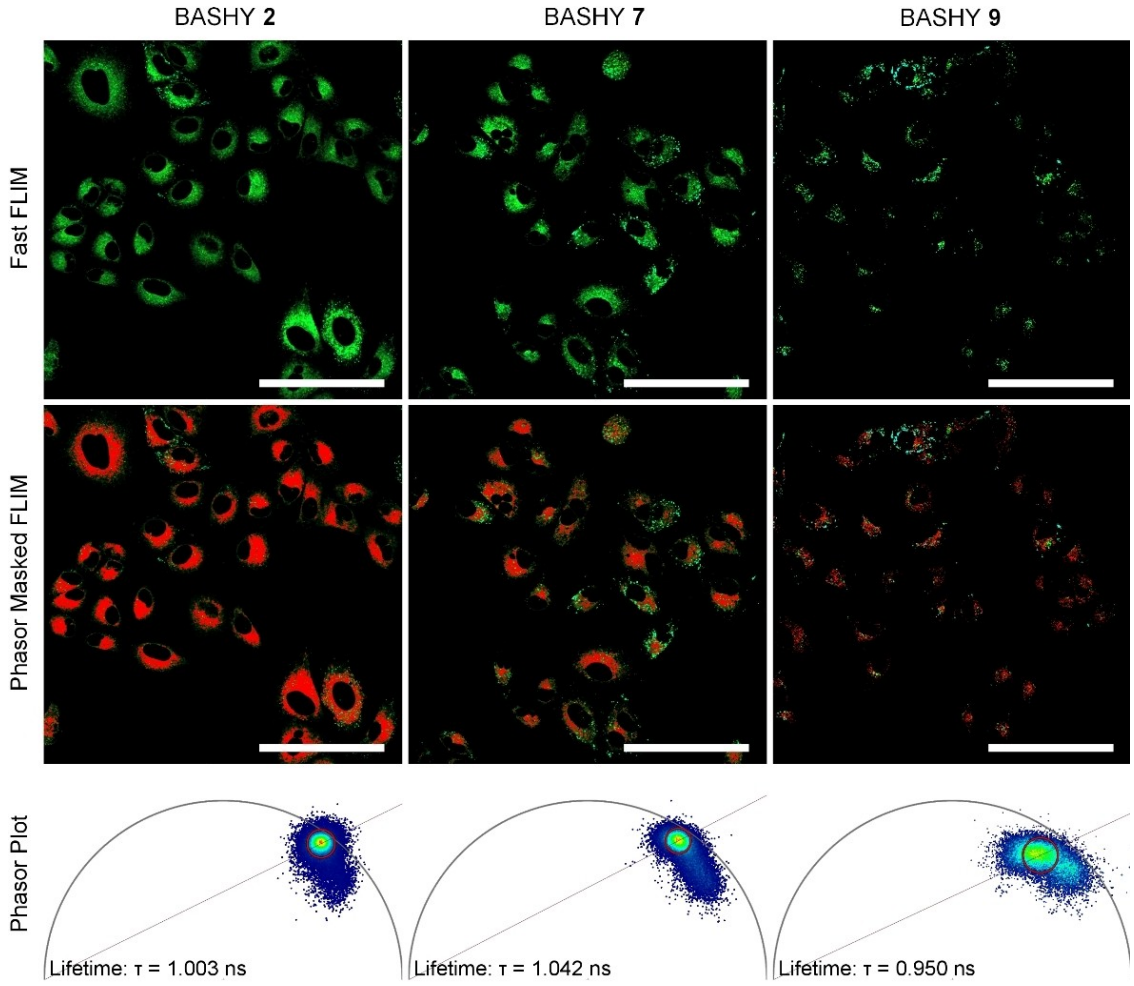

Figure 6. Top row: Fluorescence lifetime imaging (FLIM) of live A549 cells stained with the BASHY dyes (5 μM) for 4 h at 37 °C, 5% CO_2. Middle row: Phasor-separated FLIM images in which red signals represent the location of the major components that exhibit similar fluorescence lifetime within the treated cells. Bottom row: Phasor plots showing the photon population and spread of fluorescence lifetimes displayed in the FLIM images. Red circles define the major population of photons that is visualized in the phasor-separated FLIM images as red signals. Cells were imaged under physiological conditions (5% CO_2, 90% humidity, and 37 °C), excited with a 80 MHz pulsed white light laser tuned to 495 nm. Emitted photons were detected by using a HyD® X (GaAsP hybrid photocathode) detector with a filter window at 505–750 nm. Scale bar: 50 μm.

fluorescence microscopy, FLIM provides a quantitative comparison to evaluate cellular uptake efficiency as images are acquired by time-correlated single-photon counting (TCSPC) instead of by fluorescence intensity. A first inspection of the obtained images reveals that between the BASHY dyes the cellular uptake efficiency decreases with increasing conjugation length (*n*). The most prominent drop is noted for BASHY dye **9**, where $n=2$. This observation is corroborated by the fluorescence intensity images; see the Supporting Information. In addition, the increased spread on the phasor plot as *n* increases implies a greater heterogeneity of intracellular environments experienced by the dye molecules. With increasing hydrophobicity endowed by the length of *n*, these molecules are observed to be trapped in vesicles, where the different microenvironment than that within the cytosol would cause a shift in the fluorescence lifetimes to comparably smaller values. This is especially notorious for **7** and **9**. Within these cells, the major component separated by the phasor plot shows fluorescence lifetimes of about 1 ns (1.00 ns for **2**, 1.04 ns for **7**, and 0.95 ns for **9**; Figure 6), which is in rather good agreement with the data obtained from lifetime measurements in PBS (Table 3). These results confirm the photophysical integrity of the dyes in the cellular environment.

Conclusions

In conclusion, we have shown that the installation of an additional electron donor at the BASHY skeleton causes significant fluorescence quenching by means of photoinduced electron transfer (PeT) in polar organic media (especially acetonitrile). This can be harnessed for the protonation-controlled OFF-ON fluorescence switching of the dyes in organic media. However, the effect is not notable in aqueous solution, due to the deactivation of the PeT donor by hydrogen bonding with water molecules. The significant fluorescence lifetime in aqueous media (ca. 1 ns) can be employed to effectuate FLIM with the new dyes. The architectures investigated herein expand the functional scope of BASHY dyes, further unlocking their potential for application in bioimaging.

Experimental Section

General procedure for the synthesis of BASHY dyes 1–9: The synthesis was accomplished by following an adapted procedure from our earlier report.[23] In a round-bottomed flask equimolar amounts of the hydrazone (**C1**, **C2**, 1 equiv.; see structures in the Supporting Information), the α-keto carboxylic acid component (**E1**–**E3**; 1 equiv.; see structures in the Supporting Information), and the corresponding arylboronic acid (1 equiv.) were dissolved in 1 mL of CH_3CN. The reaction mixture was stirred at 80 °C for 2 h. Afterwards the volatiles were evaporated under reduced pressure and the crude mixture was re-dissolved in 1 mL of CH_2Cl_2 and purified by preparative thin layer silica gel chromatography, using CH_2Cl_2 (in the case of **1**, **2**, **6**–**9**), CH_2Cl_2/1 vol% MeOH (in the case of **3** and **4**) or CH_2Cl_2/2 vol% MeOH (in the case of **5**) as eluent.

BASHY dye 1: C1 (42 mg, 0.148 mmol), phenylglyoxylic acid (22 mg, 0.147 mmol), phenylboronic acid (18 mg, 0.148 mmol). Orange amorphous solid; 57 mg, 78% yield. ^{1}H NMR (300 MHz, $CDCl_3$): δ 7.76–7.67 (m, 2H), 7.68–7.51 (m, 4H), 7.53–7.44 (m, 2H), 7.37–7.26 (m, 2H), 7.26–7.15 (m, 1H), 6.93 (d, $J=9.3$ Hz, 1H), 6.26 (d, $J=2.4$ Hz, 1H), 6.23 (dd, $J=9.3$, 2.4 Hz, 1H), 3.61–3.23 (m, $J=7.2$ Hz, 4H), 1.22 (t, $J=7.2$ Hz, 6H); ^{13}C NMR (75 MHz, $CDCl_3$): δ 164.5, 161.8, 156.5, 155.7, 152.3, 134.9, 132.9, 130.8, 130.5, 130.4, 129.9, 129.4, 128.1, 128, 127.7, 127.6, 107.3, 107.3, 98.9, 45.21, 12.7; IR (KBr): $\nu=$ 1704 (C=O), 1617 (C=N) cm^{-1}; HRMS calcd *m/z* for $[C_{31}H_{29}BN_3O_3]^+$: 502.2296, found: 502.2288.

BASHY dye 2: C2 (60 mg, 0.169 mmol), phenylglyoxylic acid (25 mg, 0.167 mmol), phenylboronic acid (21 mg, 0.172 mmol). Red amorphous solid; 74 mg, 77% yield. ^{1}H NMR (300 MHz, $CDCl_3$): δ 7.89–7.71 (m, 2H), 7.44–7.33 (m, 4H), 7.25–7.06 (m, 7H), 6.74–6.58 (m, 2H), 6.20–6.09 (m, 2H), 3.47–3.19 (m, 8H), 1.24–1.02 (m, 12H); ^{13}C NMR (75 MHz, $CDCl_3$): δ 164.9, 161.9, 155.9, 151.2, 149.7, 135.5, 133.7, 133.5, 131, 130.2, 129.6, 129.5, 128, 127.5, 115.2, 109.9, 107.7, 106.6, 99.2, 99.1, 45.1, 44.6, 12.8, 12.6; IR (KBr): $\nu=1716$ (C=O), 1616 (C=N) cm^{-1}; HRMS calcd *m/z* for $[C_{35}H_{38}BN_4O_3]^+$: 573.3031, found: 573.3018.

BASHY dye 3: C2 (15 mg, 0.042 mmol), phenylglyoxylic acid (6.4 mg, 0.043 mmol), 4-methoxyphenylboronic acid (6.4 mg, 0.042 mmol). Red amorphous solid; 21 mg, 84% yield. ^{1}H NMR (300 MHz, $CDCl_3$): δ 7.94–7.79 (m, 2H), 7.51–7.26 (m, 7H), 7.21 (d, $J=$ 9.9 Hz, 1H), 6.89–6.65 (m, 4H), 6.35–6.12 (m, 2H), 3.72 (s, 3H), 3.64–3.31 (m, 8H), 1.33–1.15 (m, 12H); ^{13}C NMR (75 MHz, $CDCl_3$): δ 164.8, 162, 159.2, 155.9, 155.8, 151.2, 149.7, 135.5, 133.7, 133.4, 132.3, 130.3, 129.6, 128, 115.2, 113.2, 109.8, 107.7, 106.5, 99.1, 55, 45.1, 44.6, 12.8, 12.6; IR (KBr): $\nu=1718$ (C=O), 1617 (C=N) cm^{-1}; HRMS calcd *m/z* for $[C_{36}H_{40}BN_4O_4]^+$: 603.3137, found: 603.3123.

BASHY dye 4: C2 (71 mg, 0.200 mmol), phenylglyoxylic acid (30 mg, 0.200 mmol), 4-(diethylamino)phenylboronic acid (39 mg, 0.202 mmol). Red amorphous solid; 90 mg, 70% yield. ^{1}H NMR (300 MHz, $CDCl_3$): δ 7.95–7.84 (m, 2H), 7.53–7.38 (m, 2H), 7.36–7.27 (m, 5H), 7.19 (d, $J=9.3$ Hz, 1H), 6.81–6.70 (m, 2H), 6.60–6.50 (m, 2H), 6.30–6.17 (m, 2H), 3.54–3.33 (m, 8H), 3.26 (q, $J=6.9$ Hz, 4H), 1.31–1.17 (m, 12H), 1.08 (t, $J=6.9$ Hz, 6H); ^{13}C NMR (75 MHz, $CDCl_3$): δ 164.8, 162.2, 156.1, 155.7, 151.3, 149.6, 147.5, 135.4, 133.9, 133.4, 132.3, 130.1, 129.7, 128, 115.6, 111.3, 109.9, 107.9, 106.3, 99.3, 45.1, 44.6, 44.2, 12.9, 12.8, 12.7; IR (KBr): $\nu=1700$ (C=O), 1616 (C=N) cm^{-1}; HRMS calcd *m/z* for $[C_{39}H_{48}BN_5O_3]^{2+}$: 322.6920, found: 322.6912.

BASHY dye 5: C2 (53 mg, 0.150 mmol), **E3** (26 mg, 0.148 mmol), phenylboronic acid (18 mg, 0.148 mmol). Dark purple amorphous solid; 27 mg, 30% yield. ^{1}H NMR (300 MHz, $CDCl_3$): δ 8.10–7.97 (m, 2H), 7.62–7.52 (m, 2H), 7.51–7.40 (m, 4H), 7.26–7.17 (m, 4H), 6.86–6.69 (m, 2H), 6.41–6.20 (m, 2H), 3.55–3.35 (m, 8H), 1.28–1.19 (m, 12H); ^{13}C NMR (75 MHz, $CDCl_3$): δ 165.3, 162.5, 156.5, 155.4, 150, 148.1, 138.1, 135.9, 133.7, 131.7, 131, 129.9, 127, 118.8, 114.9, 113.1, 109.9, 107.2, 99.2, 45.3, 44.7, 12.9, 12.7; IR (KBr): $\nu=2227$ (CN), 1617 (C=N) cm^{-1}; HRMS calcd *m/z* for $[C_{36}H_{37}BN_5O_3]^+$: 598.2984, found: 598.2971.

BASHY dye 6: C1 (35 mg, 0.124 mmol), **E1** (22 mg, 0.125 mmol), phenylboronic acid (15 mg, 0.123 mmol). Dark purple amorphous solid; 45 mg, 70% yield. ^{1}H NMR (300 MHz, $CDCl_3$): δ 7.74–7.37 (m, 9H), 7.35–7.23 (m, 4H), 7.28–7.17 (m, 3H), 7.04 (d, $J=16.2$ Hz, 1H), 6.89 (d, $J=9.3$ Hz, 1H), 6.25 (d, $J=2.7$ Hz, 1H), 6.21 (dd, $J=9.3$, 2.7 Hz, 1H), 3.62–3.23 (m, 4H), 1.22 (t, $J=7.2$ Hz, 6H); ^{13}C NMR (75 MHz, $CDCl_3$): δ 164, 161.8, 156.3, 150.6, 138.9, 136.2, 134.8, 130.9, 130.3, 130.2, 129.4, 128.7, 128.1, 127.7, 121.2, 107.8, 107.3, 99, 45.3, 12.8; IR (KBr): $\nu=1703$ (C=O), 1614 (C=N) cm^{-1}; HRMS calcd *m/z* for $[C_{33}H_{31}BN_3O_3]^+$: 528.2453, found: 528.2444.

BASHY dye 7: C2 (35 mg, 0.099 mmol), **E1** (17 mg, 0.096 mmol), phenylboronic acid (12 mg, 0.098 mmol). Dark purple amorphous solid; 49 mg, 85% yield. ^{1}H NMR (300 MHz, $CDCl_3$): δ 7.62 (d, $J=$

16.5 Hz, 1H), 7.49–7.40 (m, 6H), 7.35–7.27 (m, 3H), 7.25–7.17 (m, 4H), 7.13 (d, J = 16.5 Hz, 1H), 6.84–6.70 (m, 2H), 6.31–6.16 (m, 2H), 3.72–3.20 (m, 8H), 1.30–1.18 (m, 12H); ^{13}C NMR (75 MHz, $CDCl_3$): δ 164.3, 161.9, 156.5, 155.8, 149.7, 149.3, 138.1, 136.5, 135.5, 133.6, 131, 129.1, 128.7, 127.7, 127.5, 121.7, 115.3, 109.8, 108.1, 106.6, 99.2, 99.1, 45.1, 44.6, 12.8, 12.7; IR (KBr): ν = 1710 (C=O), 1633 (C=N) cm^{-1}; HRMS calcd m/z for $[C_{37}H_{40}BN_4O_3]^+$: 599.3188, found: 599.3174.

BASHY dye 8: C1 (35 mg, 0.124 mmol), **E2** (25 mg, 0.124 mmol), phenylboronic acid (15 mg, 0.123 mmol). Dark purple amorphous solid; 41 mg, 60% yield. ^{1}H NMR (300 MHz, $CDCl_3$): δ 7.67–7.50 (m, 4H), 7.49–7.42 (m, 2H), 7.42–7.36 (m, 2H), 7.35–7.27 (m, 4H), 7.25–7.16 (m, 4H), 6.88 (d, J = 9.3 Hz, 1H), 6.84–6.55 (m, 3H), 6.24 (d, J = 2.4 Hz, 1H), 6.20 (dd, J = 9.3, 2.4 Hz, 1H), 3.62–3.13 (m, 4H), 1.21 (t, J = 7.2 Hz, 6H); ^{13}C NMR (75 MHz, $CDCl_3$): δ 163.8, 161.8, 156.4, 156.3, 150.7, 139.7, 138.2, 136.8, 134.8, 130.9, 130.3, 130.3, 128.9, 128.8, 128.6, 127.7, 127.7, 127, 125.4, 107.9, 107.2, 99.1, 45.3, 12.9; IR (KBr): ν = 1704 (C=O), 1616 (C=N) cm^{-1}; HRMS calcd m/z for $[C_{35}H_{33}BN_3O_3]^+$: 554.2609, found: 554.2603.

BASHY dye 9: C2 (40 mg, 0.113 mmol), **E2** (23 mg, 0.114 mmol), phenylboronic acid (14 mg, 0.115 mmol). Dark purple amorphous solid; 56 mg, 80% yield. ^{1}H NMR (300 MHz, $CDCl_3$): δ 7.51–7.34 (m, 7H), 7.37–7.26 (m, 2H), 7.27–7.12 (m, 5H), 6.95–6.61 (m, 5H), 6.27–6.18 (m, 2H), 3.56–3.31 (m, 8H), 1.28 (t, J = 7.2 Hz, 6H), 1.21 (t, J = 7.2 Hz, 6H); ^{13}C NMR (75 MHz, $CDCl_3$): δ 138.8, 137.5, 136.9, 135.4, 133.6, 131, 129.1, 128.8, 128.5, 127.5, 126.9, 125.9, 115.4, 109.8, 108.2, 106.6, 99.2, 45.1, 44.6, 12.8, 12.7; IR (KBr): ν = 1700 (C=O), 1615 (C=N) cm^{-1}; HRMS calcd m/z for $[C_{39}H_{42}BN_4O_3]^+$: 625.3344, found: 625.3331.

Photophysical measurements: All measurements were done in quartz cuvettes (1 cm optical pathlength) and at room temperature (23 °C). UV/vis absorption spectra were registered on a Cary 50 UV/Vis spectrophotometer (Varian) and corrected fluorescence spectra were measured with a Varian Cary Eclipse fluorimeter with a pulsed Xenon lamp as excitation source. Lifetime measurements were performed using a time-correlated single-photon-counting instrument (Edinburgh Instruments FLS 920). For this purpose, samples were excited with a picosecond-pulsed EPLED 485 (482.0 nm, pulse width FWHM: 100.6 ps). A light-scattering Ludox solution was used to obtain the instrument response function, used in the deconvolution fitting of the kinetic decay curves. The emission quantum yields were measured for optically diluted solutions (A ca. 0.1 at the excitation wavelength) and relative to *N*-propyl-4-amino-1,8-naphthalimide (Φ_f = 0.48 in aerated acetonitrile).[23] Eventually different refractive indices of the solvents of the simple and reference were taken into account.[40]

Transient absorption experiments were performed using an OPO System Ekspla (EKS-NT342C-10) coupled with an UV extension (EKS-NT342C-SH-SFG) as the excitation source and an Edinburgh Instruments detection system (LP980) coupled with an ICCD camera (Andor iStar CCD 320T). Optically diluted samples (A ca. 0.1 at excitation wavelength) in acetonitrile were used. Information on the excitation wavelengths is included in the main text (see above).

Phasor fluorescence lifetime imaging microscopy (phasor-FLIM): A549 cells were seeded at a density of 20000 cells per well in DMEM (10% FBS, 1% penicillin/streptomycin) within an IBIDI 8-well confocal slide. After adhering for 24 h, cells were treated with the BASHY **2**, **7**, and **9** for 4 h at 37 °C, 5% CO_2. The samples were dissolved in DMSO at a concentration of 10 mM and diluted to a final volume of 400 μL with DMEM. Sample solutions were further diluted to an end concentration of 5 μM with DMEM and added to the cells (total DMSO content = 0.05 vol%) after aspiration. After incubation, cells were washed twice with DMEM and imaged live. Cells were imaged under physiological conditions using an incubator-equipped Leica Stellaris 8 microscope (40×glycerol objective, HC PL APO CS2 40×/1.25 GLYC) with fast lifetime contrast (FALCON) module (Leica Microsystem GmbH). The incubator (okolab) is set and held constant at 37 °C, 5% CO_2 and a relative humidity of 90% throughout all measurements. Samples were excited using a 80 MHz pulse white light laser tuned to 495 nm for both intensity and fluorescence lifetime measurements. Emitted photons were detected using HyD® X (GaAsP hybrid photocathode) detector with a filter window at 505–750 nm. The IRF standard used is fluorescein sodium salt.

Fluorescence lifetime imaging (FLIM) was conducted with living cells with a scanning resolution of 1024×1024 pixels at 400 Hz and 5 frame repetitions for each image. Photons were counted based on FALCON-modified time correlated single photon counting (TCSPC). Each pixel is transformed into a phasor plot according to the following equation:

$$g_{i,j}(\omega) = \int_0^T I(t) \cdot \cos(n\omega t)\mathrm{d}t \Big/ \int_0^T I(t)\mathrm{d}t$$

$$s_{i,j}(\omega) = \int_0^T I(t) \cdot \sin(n\omega t)\mathrm{d}t \Big/ \int_0^T I(t)\mathrm{d}t$$

in which $g_{i,j}(\omega)$ and $s_{i,j}(\omega)$ are the x and y coordinates of the phasor plot, n and ω are the harmonic frequency and the angular frequency of excitation, respectively, and T is the repeat frequency of the acquisition. Frequency domain data acquisition from each pixel can be converted to phasor points using the following transformations:

$$g_{i,j}(\omega) = m_{i,j} \cdot \cos\left(\phi_{i,j}\right)$$

$$s_{i,j}(\omega) = m_{i,j} \cdot \sin\left(\phi_{i,j}\right)$$

in which $m_{i,j}$ and $\varphi_{i,j}$ are the modulation and phase shift, respectively, of the frequency domain measurement at pixel i,j. The decay from each pixel can hence be translated to a point in the phasor plot.[41] Phasor components were identified and separated using LAS X software. Photons that are out of the defined phasor are excluded from the images.

Theoretical calculations: All calculations were carried out with the Gaussian 16 package.[42] The solvent effects were taken into account by the polarizable continuum model (PCM),[43] considering acetonitrile as solvent. For all molecules, the ground state geometry optimization was performed using the long-range-corrected LC-wHPBE hybrid functional[37] with the 6-31G(d) basis set. All the structures obtained were confirmed as true minima by the absence of a negative frequency in the vibrational analysis. The photophysical properties were computed as vertical electronic excitations from the minima of the ground-state, using the linear-response approach, the same functional, the larger basis set 6-311++G(2d,p) and computing the first ten excited states. The Natural transition orbital (NTO) calculations[39] were performed after TD-DFT calculations to describe the physical behavior of the holes and the electrons in excited states. Finally, the charge transfer indices were obtained using the Multifunctional Wavefunction Analyzer (MULTIWFN version 3.6).[44]

Acknowledgements

This work was generously supported by the Portuguese Fundação para a Ciência e Tecnologia [grants PTDC/QUI-OUT/3989/2021 (P.G.); institutional grants UIDB/04138/2020 and UIDP/04138/2020 (iMed)], the Spanish Ministerio de Ciencia e Innovación [grants CTQ2017-89832-P, PID2020-119992GB-I00 (both to U.P.), and PID2019-104293GB-I00 (F.N.)], the Consejería de Universidad, Investigación e Innovación/Junta de Andalucía [grant P18-FR-4080 (U.P.)], and the Universidad de Huelva/Junta de Andalucía [UHU202070 (U.P.)]. The NMR spectrometers are part of the Portuguese National NMR Network (PT NMR) and are partially supported by Infrastructure Project No. 022161 (co-financed by FEDER through COMPETE 2020, POCI, PORL, and FCT through PIDDAC). We also acknowledge the Supercomputing and Bioinformatics Centre (SCBI) of the University of Málaga for providing the computer resources used for the theoretical calculations.

Conflict of Interest

The authors declare no conflict of interest.

Data Availability Statement

The data that support the findings of this study are available from the corresponding author upon reasonable request.

Keywords: charge transfer · electron transfer · fluorescence · fluorescence lifetime imaging · organoboron dyes

[1] A. Loudet, K. Burgess, *Chem. Rev.* **2007**, *107*, 4891.
[2] G. Ulrich, R. Ziessel, A. Harriman, *Angew. Chem. Int. Ed.* **2008**, *47*, 1184.
[3] M. Beija, C. A. M. Afonso, J. M. G. Martinho, *Chem. Soc. Rev.* **2009**, *38*, 2410.
[4] M. Vendrell, D. Zhai, J. C. Er, Y.-T. Chang, *Chem. Rev.* **2012**, *112*, 4391.
[5] J. B. Grimm, A. J. Sung, W. R. Legant, P. Hulamm, S. M. Matlosz, E. Betzig, L. D. Lavis, *ACS Chem. Biol.* **2013**, *8*, 1303.
[6] L. D. Lavis, R. T. Raines, *ACS Chem. Biol.* **2014**, *9*, 855.
[7] X. Li, X. Gao, W. Shi, H. Ma, *Chem. Rev.* **2014**, *114*, 590.
[8] T. Kowada, H. Maeda, K. Kikuchi, *Chem. Soc. Rev.* **2015**, *44*, 4953.
[9] Y. Kushida, T. Nagano, K. Hanaoka, *Analyst* **2015**, *140*, 685.
[10] W. Xu, Z. Zeng, J.-H. Jiang, Y.-T. Chang, L. Yuan, *Angew. Chem. Int. Ed.* **2016**, *55*, 13658.
[11] A. S. Klymchenko, *Acc. Chem. Res.* **2017**, *50*, 366.
[12] L. D. Lavis, *Biochemistry* **2017**, *56*, 5165.
[13] D. Frath, J. Massue, G. Ulrich, R. Ziessel, *Angew. Chem. Int. Ed.* **2014**, *53*, 2290.
[14] S. Kolemen, M. Işık, G. M. Kim, D. Kim, H. Geng, M. Buyuktemiz, T. Karatas, X.-F. Zhang, Y. Dede, J. Yoon, E. U. Akkaya, *Angew. Chem. Int. Ed.* **2015**, *54*, 5340.
[15] V. F. Pais, M. M. Alcaide, R. López-Rodríguez, D. Collado, F. Nájera, E. Pérez-Inestrosa, E. Álvarez, J. M. Lassaletta, R. Fernández, A. Ros, U. Pischel, *Chem. Eur. J.* **2015**, *21*, 15369.
[16] S. P. J. T. Bachollet, D. Volz, B. Fiser, S. Münch, F. Rönicke, J. Carrillo, H. Adams, U. Schepers, E. Gómez-Bengoa, S. Bräse, J. P. A. Harrity, *Chem. Eur. J.* **2016**, *22*, 12430.
[17] L. Ji, S. Griesbeck, T. B. Marder, *Chem. Sci.* **2017**, *8*, 846.
[18] K. Liu, R. A. Lalancette, F. Jäkle, *J. Am. Chem. Soc.* **2017**, *139*, 18170.
[19] Z. Domínguez, R. López-Rodríguez, E. Álvarez, S. Abbate, G. Longhi, U. Pischel, A. Ros, *Chem. Eur. J.* **2018**, *24*, 12660.
[20] J. Full, S. P. Panchal, J. Götz, A.-M. Krause, A. Nowak-Krll, *Angew. Chem. Int. Ed.* **2021**, *60*, 4350.
[21] M. Vanga, A. Sahoo, R. A. Lalancette, F. Jäkle, *Angew. Chem. Int. Ed.* **2022**, *61*, e202113075.
[22] T. Yang, A. Valavalkar, A. Romero-Arenas, A. Dasgupta, P. Then, A. Chettri, C. Eggeling, A. Ros, U. Pischel, B. Dietzek-Ivanšić, *Chem. Eur. J.* **2023**, *29*, e202203468.
[23] F. M. F. Santos, J. N. Rosa, N. R. Candeias, C. Parente Carvalho, A. I. Matos, A. E. Ventura, H. F. Florindo, L. C. Silva, U. Pischel, P. M. P. Gois, *Chem. Eur. J.* **2016**, *22*, 1631.
[24] M. M. Alcaide, F. M. F. Santos, V. F. Pais, J. I. Carvalho, D. Collado, E. Pérez-Inestrosa, J. F. Arteaga, F. Boscá, P. M. P. Gois, U. Pischel, *J. Org. Chem.* **2017**, *82*, 7151.
[25] A. D. Laurent, B. L. Guennic, D. Jacquemin, *Theor. Chem. Acc.* **2016**, *135*, 173.
[26] F. M. F. Santos, Z. Domínguez, J. P. L. Fernandes, C. Parente Carvalho, D. Collado, E. Pérez-Inestrosa, M. V. Pinto, A. Fernandes, J. F. Arteaga, U. Pischel, P. M. P. Gois, *Chem. Eur. J.* **2020**, *26*, 14064.
[27] P. M. S. D. Cal, F. Sieglitz, F. M. F. Santos, C. Parente Carvalho, A. Guerreiro, J. B. Bertoldo, U. Pischel, P. M. P. Gois, G. J. L. Bernardes, *Chem. Commun.* **2017**, *53*, 368.
[28] B. Zhang, G. Feng, S. Wang, X. Zhang, *Dyes Pigm.* **2017**, *149*, 356.
[29] M. V. Pinto, F. M. F. Santos, C. Barros, A. R. Ribeiro, U. Pischel, P. M. P. Gois, A. Fernandes, *Cells* **2021**, *10*, 3163.
[30] B. Tang, F. Yu, P. Li, L. Tong, X. Duan, T. Xie, X. A. Wang, *J. Am. Chem. Soc.* **2009**, *131*, 3016.
[31] J. Han, K. Burgess, *Chem. Rev.* **2010**, *110*, 2709.
[32] W. Sun, S. Guo, C. Hu, J. Fan, X. Peng, *Chem. Rev.* **2016**, *116*, 7768.
[33] T. Flagstad, M. T. Petersen, T. E. Nielsen, *Angew. Chem. Int. Ed.* **2015**, *54*, 8395.
[34] L. Levi, T. J. J. Müller, *Chem. Soc. Rev.* **2016**, *45*, 2825.
[35] F. de Moliner, N. Kielland, R. Lavilla, M. Vendrell, *Angew. Chem. Int. Ed.* **2017**, *56*, 3758.
[36] R. V. Bensasson, J.-C. Gramain, *J. Chem. Soc. Faraday Trans. 1* **1980**, *76*, 1801.
[37] T. M. Henderson, A. F. Izmaylov, G. Scalmani, G. E. Scuseria, *J. Chem. Phys.* **2009**, *131*, 044108.
[38] C. A. Guido, P. Cortona, B. Mennucci, C. Adamo, *J. Chem. Theory Comput.* **2013**, *9*, 3118.
[39] R. L. Martin, *J. Chem. Phys.* **2003**, *118*, 4775.
[40] B. Valeur, M. N. Berberan-Santos, *Molecular Fluorescence: Principles and Applications*, 2nd ed., Wiley-VCH, Weinheim, **2012**.
[41] S. Ranjit, L. Malacrida, D. M. Jameson, E. Gratton, *Nat. Protoc.* **2018**, *13*, 1979.
[42] Gaussian 16, Revision C.01, M. J. Frisch, G. W. Trucks, H. B. Schlegel, G. E. Scuseria, M. A. Robb, J. R. Cheeseman, G. Scalmani, V. Barone, G. A. Petersson, H. Nakatsuji, X. Li, M. Caricato, A. V. Marenich, J. Bloino, B. G. Janesko, R. Gomperts, B. Mennucci, H. P. Hratchian, J. V. Ortiz, A. F. Izmaylov, J. L. Sonnenberg, D. Williams-Young, F. Ding, F. Lipparini, F. Egidi, J. Goings, B. Peng, A. Petrone, T. Henderson, D. Ranasinghe, V. G. Zakrzewski, J. Gao, N. Rega, G. Zheng, W. Liang, M. Hada, M. Ehara, K. Toyota, R. Fukuda, J. Hasegawa, M. Ishida, T. Nakajima, Y. Honda, O. Kitao, H. Nakai, T. Vreven, K. Throssell, J. A. Montgomery, Jr., J. E. Peralta, F. Ogliaro, M. J. Bearpark, J. J. Heyd, E. N. Brothers, K. N. Kudin, V. N. Staroverov, T. A. Keith, R. Kobayashi, J. Normand, K. Raghavachari, A. P. Rendell, J. C. Burant, S. S. Iyengar, J. Tomasi, M. Cossi, J. M. Millam, M. Klene, C. Adamo, R. Cammi, J. W. Ochterski, R. L. Martin, K. Morokuma, O. Farkas, J. B. Foresman, D. J. Fox, Gaussian, Inc., Wallingford CT, **2016**.
[43] J. Tomasi, B. Mennucci, R. Cammi, *Chem. Rev.* **2005**, *105*, 2999.
[44] T. Lu, F. W. Chen, *J. Comput. Chem.* **2012**, *33*, 580.

Manuscript received: February 21, 2023
Accepted manuscript online: March 27, 2023
Version of record online: April 19, 2023